Electronic Supplementary Information

Aggregation-induced Heterogeneities in the Emission of Upconverting Nanoparticles at the Submicron Scale Unfolded by Hyperspectral Microscopy

Francisco Gonell,[ab¥] Alexandre M. P. Botas,[c¥] Carlos D. S. Brites,[c] Pedro Amoros,[d] Luís D. Carlos,[*c] Beatriz Julián-López[*a] and Rute A. S. Ferreira[*c]

[a]Institute of Advanced Materials (INAM), Universitat Jaume I, Castellón de la Plana, 12006, Spain. E-mail: julian@uji.es
[b]Current address: Laboratoire de Chimie de la Matière Condensée de Paris (LCMCP), Sorbonne Université, CNRS, Collège de France, Paris, 75005, France
[c]Department of Physics and CICECO — Aveiro Institute of Materials, University of Aveiro Aveiro, 3810-193, Portugal. E-mail: rferreira@ua.pt, lcarlos@ua.pt
[d]Institute of Materials Science (ICMUV), University of Valencia, Catedrático José Beltrán 2, 46980 Paterna, Valencia, Spain

[¥] These authors contributed equally to this work.

Contents

1. Structural characterization

X-ray diffraction (XRD)

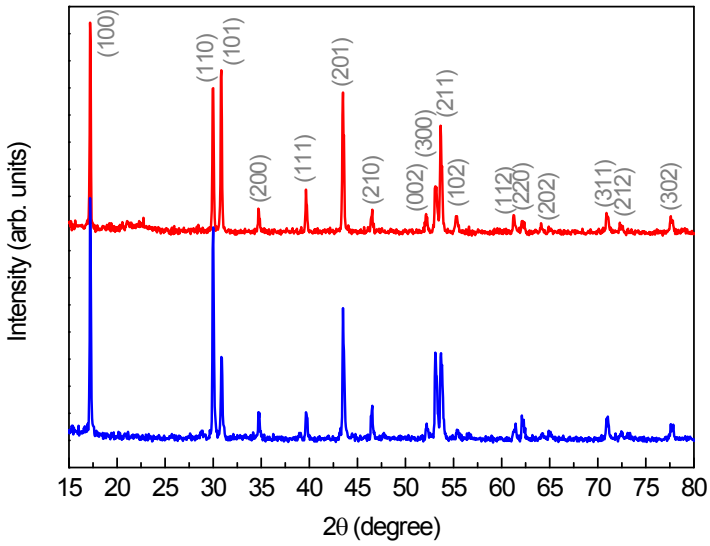

Figure S1. Powder XRD diffractograms of as-synthesized (red) α-$NaYF_4$:Yb^{3+}/Er^{3+} and (blue) α-$NaYF_4$:Yb^{3+}/Tm^{3+} UCNPs. The experimental peaks are assigned to the crystalline planes (ICDD Nr 28-1192).

Scanning transmission electron microscope (STEM)

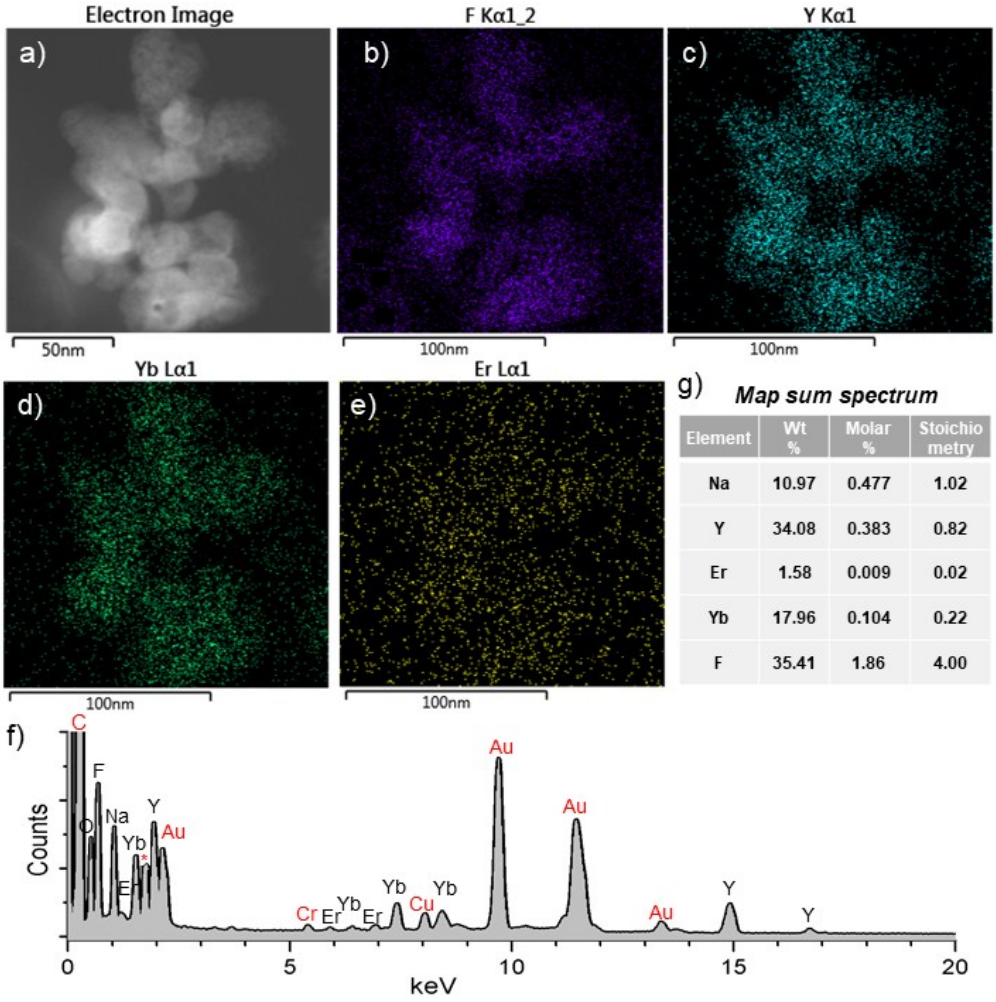

g) ***Map sum spectrum***

Element	Wt %	Molar %	Stoichiometry
Na	10.97	0.477	1.02
Y	34.08	0.383	0.82
Er	1.58	0.009	0.02
Yb	17.96	0.104	0.22
F	35.41	1.86	4.00

Figure S2. a) High-angle annular dark-field image (HAADF)- STEM Image and b-e) images of local elemental mapping by energy dispersive X-ray analysis (EDX) line scans for $NaYF_4$:Er^{3+}/Yb^{3+} crystals. f) EDX analysis of elemental composition from the region analyzed in the mapping (map sum spectrum). The elements depicted in red correspond to the gold grids and their carbon films, as well as traces of copper and chromium from the microscope instrument (holder and lenses). g) Table with the elemental percentages in weight, in moles (wt/atomic mass) and calculated stoichiometry, which fits well with the theoretical formula $NaY_{0.78}Er_{0.02}Yb_{0.2}F_4$.

2. UV/visible/NIR absorbance

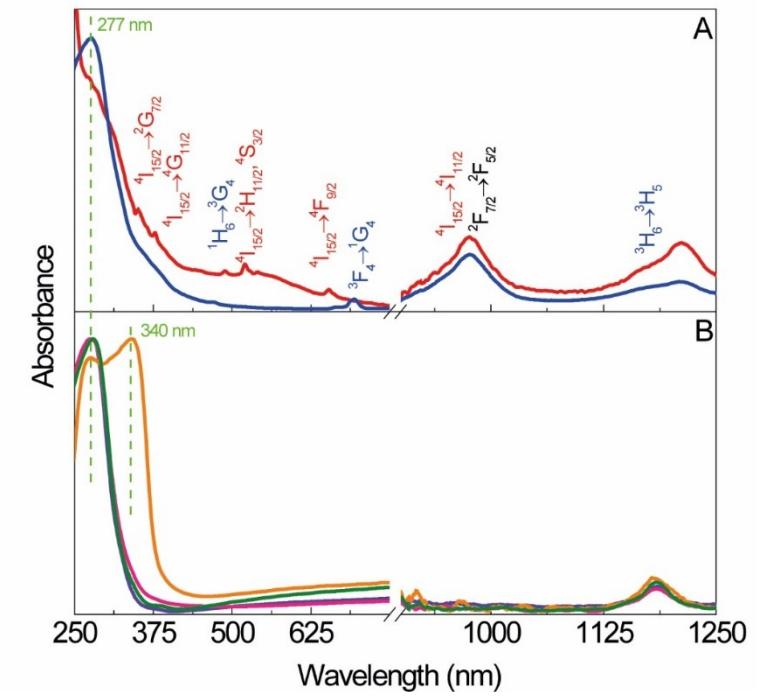

Figure S3. UV/visible/NIR abosrnbance spectra of: (A) $NaYF_4:Yb^{3+}/Er^{3+}$ (red) and $NaYF_4:Yb^{3+}/Tm^{3+}$ (blue) UCNPs and (B) hybrid monoliths (green) HyNb, (pink) HyTa, (violet) HyZr, and (orange) HyTi embedding the $NaYF_4:Yb^{3+}/Er^{3+}$ UCNPs. The Er^{3+} (in red), Tm^{3+} (in blue) and Yb^{3+} (in black) transitions are identified in (A).

3. Upconversion emission

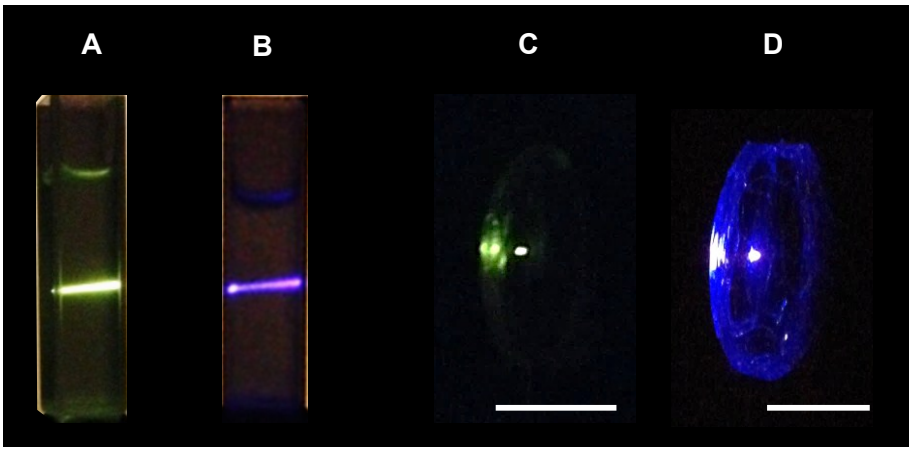

Figure S4. Photographs of the upconversion emission in cyclohexane suspensions of (A) $NaYF_4$:Yb^{3+}/Er^{3+} and (B) $NaYF_4$:Yb^{3+}/Tm^{3+} and of the monoliths HyTa embedding the (C) $NaYF_4$:Yb^{3+}/Er^{3+} and the (D) $NaYF_4$:Yb^{3+}/Tm^{3+} NPs (λ_{exc} 980 nm, 1.5±0.1 W·cm^{-2}). The cuvettes length is 10 mm and the scale bars in (C) and (D) correspond to 20 mm.

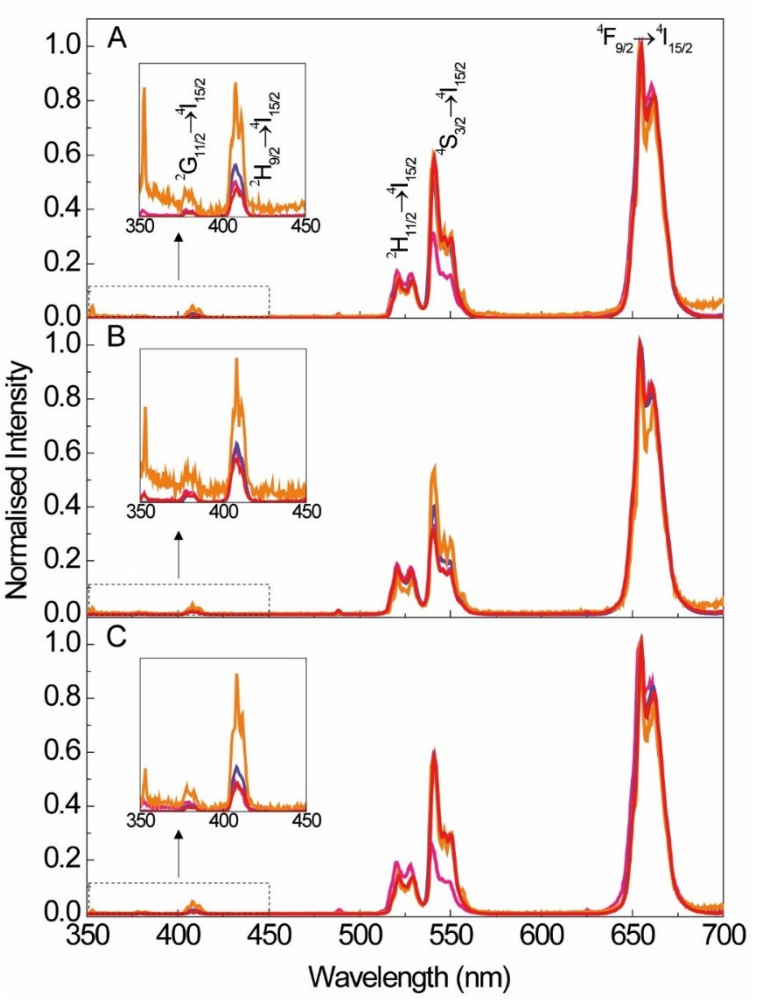

Figure S5. Room temperature upconversion emission spectra of (A) HyNb-Yb^{3+}/Er^{3+}, (B) HyTi-Yb^{3+}/Er^{3+} and (C) HyZr-Yb^{3+}/Er^{3+} hybrids processed as monolith (violet), film (orange) and grinded monolith (pink). In the three pictures, the upconversion emission of the pure UCNPs (red) is included for comparison. The insets show magnifications of the 350-450 nm range. The Er^{3+} transitions are identified in (A).

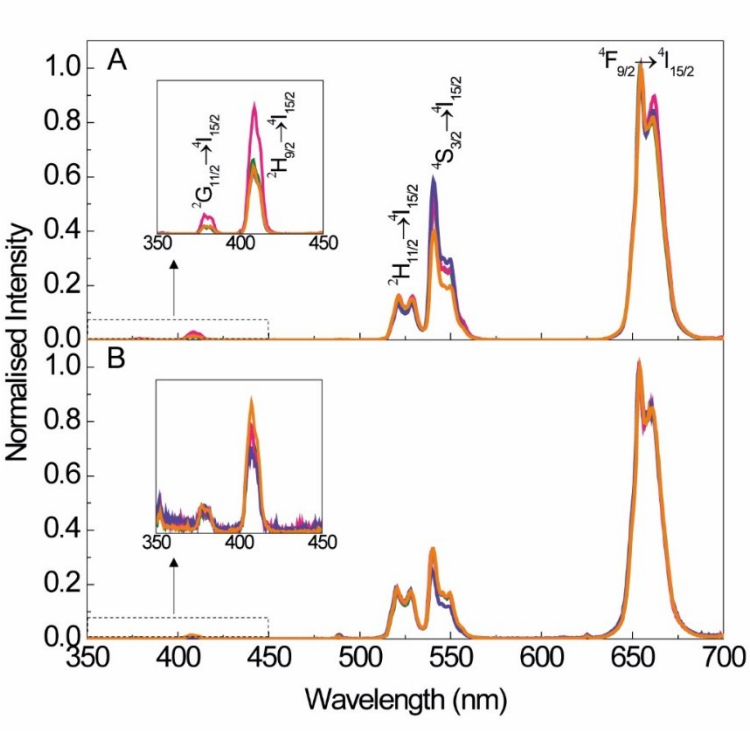

Figure S6. Room temperature upconversion emission spectra of HyNb-Yb^{3+}/Er^{3+}(green), HyTa-Yb^{3+}/Er^{3+} (pink), HyZr-Yb^{3+}/Er^{3+} (violet) and HyTi-Yb^{3+}/Er^{3+} (orange) processed as (A) monoliths and (B) grinded monoliths recorded at a laser power of 128.5 W/cm^2. The insets show magnifications of the 350-450 nm range. The Er^{3+} transitions are identified in (A).

4. Emission spectra as function of the laser power density

The number of photons involved in the upconverting process was determined from the green ($^2H_{11/2}\rightarrow{}^4I_{15/2}$ and $^4S_{3/2}\rightarrow{}^4I_{15/2}$) and red ($^4F_{9/2}\rightarrow{}^4I_{15/2}$) integrated intensity with the excitation power density for the hybrid materials. In general, the number of photons, *N*, required to populate the upper emitting state, under unsaturated conditions, can be determined by the power-like relation between the excitation intensity, I_{exc}, and the emitted integrated power, P_{emi}, expressed as $P_{emi} \propto I_{exc}{}^N$.[1] A *log-log* plot of the emitted integrated intensity vs excitation intensity result (for low excitation powers) in a straight line with slope equal to the mean number of photons involved in the process.

The power-dependence measurements were performed for the pure UCNPs and the hybrid nanocomposites, and the results are illustrated in Fig. S6 (HyTa-Yb^{3+}/Er^{3+}) and Fig. S7 (HyZr-Yb^{3+}/Er^{3+}, HyTi-Yb^{3+}/Er^{3+} and HyNb-Yb^{3+}/Er^{3+} hybrids). After the appropriate analysis, the slope obtained from the fittings were close to 2 (Table S1), demonstrating that both red and green emissions were the result of a two-photon upconversion process. Interestingly, the R/G integrated intensity ratio is rather constant with the excitation laser powder density (Fig. S8) in good concordance with the results of similar $NaYF_4$:Yb^{3+}/Er^{3+} materials.[2] Table S2 resumes the number of photons involved in the upconversion process determined for the blue ($^1G_4\rightarrow{}^3H_6$)

and red ($^3F_3 \rightarrow {}^3H_6$) integrated intensity with the excitation power density using the strategy described for the Yb^{3+}/Er^{3+}-doped hybrid.

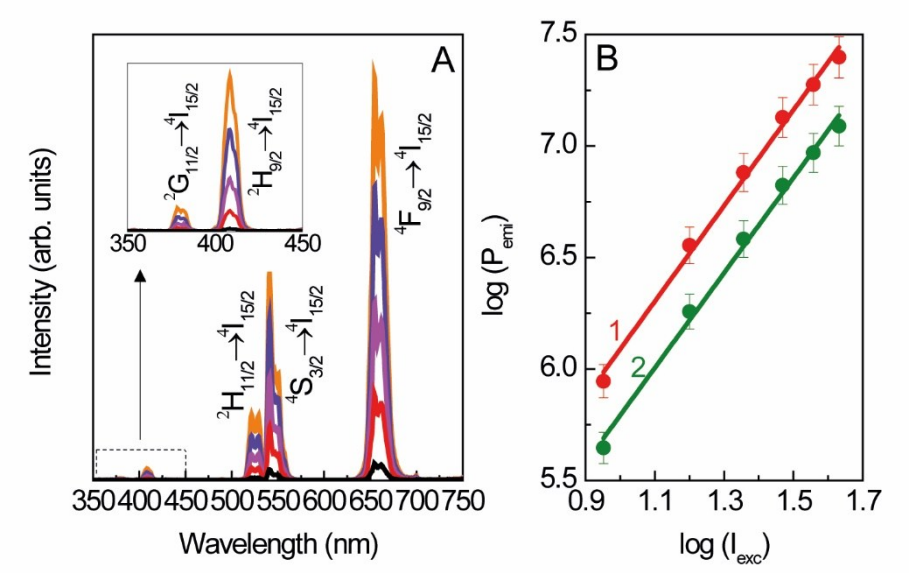

Figure S7. (A) Spectral power of HyTa-Yb^{3+}/Er^{3+} upon different excitation power densities: (black) 15.9, (red) 36.1, (magenta) 55.8, (violet) 81.1 and (orange) 128.2 $W \cdot cm^{-2}$. The inset shows the magnification of the 350-450 nm wavelength region. (B) Log-log plot of the P_{emi} of the (2) green ($^2H_{11/2}$, $^2S_{3/2} \rightarrow {}^4I_{15/2}$) and (1) red ($^4F_{9/2} \rightarrow {}^4I_{15/2}$) transitions with the I_{exc} resulting from the integration of the spectral power in the ranges 500-580 nm and 620-710 nm respectively.

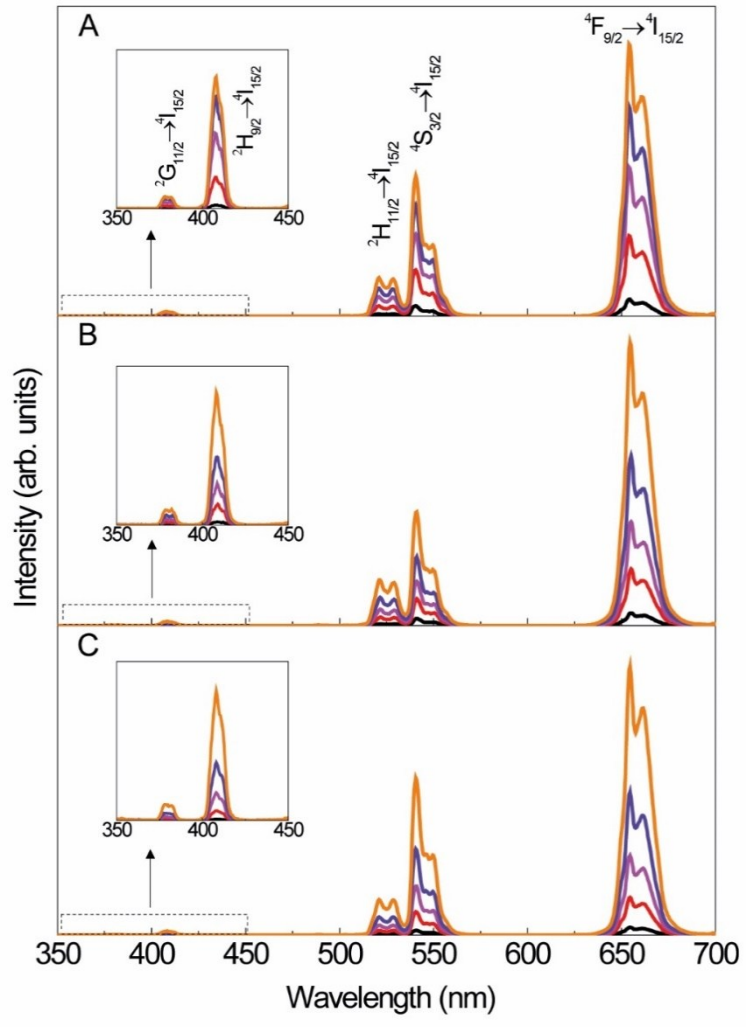

Figure S8. Dependence of the upconversion emission with the excitation power density of (black) 15.9, (red) 36.1, (magenta) 55.8, (violet) 81.1 and (orange) 128.2 W.cm^{-2}, for (A) HyNb-Yb^{3+}/Er^{3+}, (B) HyTi-Yb^{3+}/Er^{3+} and (C) HyZr-Yb^{3+}/Er^{3+} nanocomposites. The insets show magnifications of the 350-450 nm range. The Er^{3+} transitions are identified in (A).

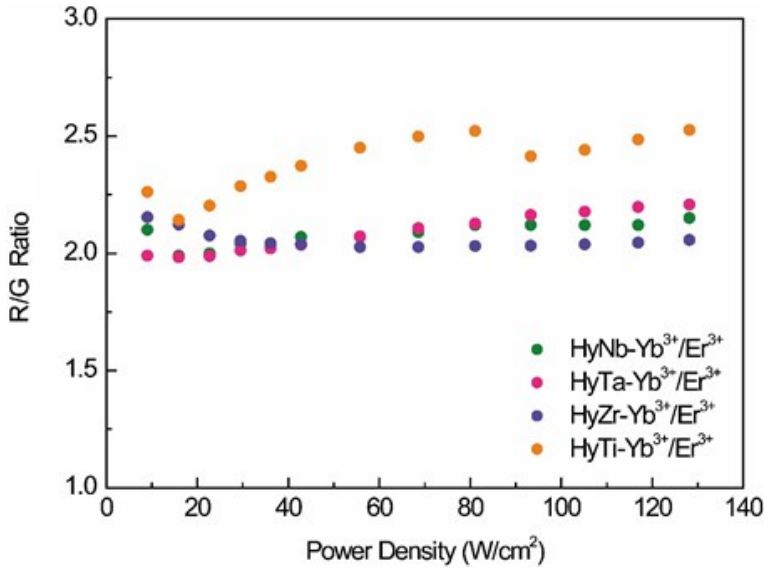

Figure S9. Dependence with the power density of the R/G ratio of the upconversion emissions of HyM-Yb^{3+}/Er^{3+} nanocomposites.

Table S1. Slopes from the dependence of the integrated emitted power (P_{em})with the excitation laser intensity (I_{exc}) for $NaYF_4$:Yb^{3+}/Er^{3+} UCNPs and HyM-Yb^{3+}/Er^{3+} hybrids.

	$^2H_{11/2}$, $^4S_{3/2}\rightarrow{}^4I_{15/2}$	$^4F_{9/2}\rightarrow{}^4I_{15/2}$
$NaYF_4$-Yb^{3+}/Er^{3+}	1.8	1.8
HyNb	1.6	1.6
HyTa	1.8	1.9
HyTi	2.0	2.0
HyZr	1.7	1.7

Table S2. Slopes from the dependence of the P_{em} with I_{exc} for $NaYF_4$:Tm^{3+}/Yb^{3+} UCNPs and the HyM-Tm^{3+}/Yb^{3+} hybrids.

	$^1G_4\rightarrow{}^3H_6$	$^3F_3\rightarrow{}^3H_6$
$NaYF_4$-Yb^{3+}/Tm^{3+}	3.13	2.60
HyNb	1.80	1.60
HyTa	1.63	1.66
HyTi	1.23	1.22
HyZr	1.73	1.47

References

1. G. Chen, T. Y. Ohulchanskyy, R. Kumar, H. Ågren and P. N. Prasad, *ACS Nano*, 2010, **4**, 3163-3168.
2. H.-X. Mai, Y.-W. Zhang, L.-D. Sun and C.-H. Yan, *J. Phys. Chem. C*, 2007, **111**, 13721-13729.